Heliyon 8 (2022) e10043

Contents lists available at ScienceDirect

Heliyon

journal homepage: www.cell.com/heliyon

Research article

# Noninvasive imaging of the lung NETosis by anti-Ly6G iron oxide nanoparticles

Jianghong Zhong [a,b,**], Chanyu Zheng [c], Haiqiang Gao [c], Wei Tong [d], Hui Hui [d], Jie Tian [a,b,d,*,1]

[a] School of Engineering Medicine, Beihang University, Beijing 100191, China
[b] Key Laboratory of Big Data-Based Precision Medicine (Beihang University), Ministry of Industry and Information Technology, Beijing, 100191, China
[c] School of Biological Science and Medical Engineering, Beihang University, Beijing 100191, China
[d] CAS Key Laboratory of Molecular Imaging, Beijing Key Laboratory of Molecular Imaging, The State Key Laboratory of Management and Control for Complex Systems, Institute of Automation, Chinese Academy of Sciences, Beijing 100190, China

ARTICLE INFO

*Keywords:*
Neutrophil
NET
Iron oxide nanoparticle
Magnetic particle imaging
Lupus

ABSTRACT

It is challenging to visualize noninvasively the formation of neutrophil extracellular traps, known as NETosis, and therefore difficult to monitor disease progression. A desirable molecular imaging probe is the iron oxide nanoparticle (NP) that could induce reactive oxygen species. Here, we used C57BL/6 mice with pristane-induced lupus, which mimics systemic lupus erythematosus. Administration of anti-Ly6G antibody-conjugated NP allowed detection of NETosis with fluorescent molecular imaging, as evidenced by flow cytometric analysis of citrullinated histone H3 expression in lung neutrophils. This finding was consistent with NP-induced blood NETosis in a spontaneous lupus model of B6.MRL-*lpr* mice. *A chronic* assessment was performed in which the lupus mice were protected from enhanced oxidative burst by anti-Ly6G NP. This NP can migrate from the peritoneal cavity to the lungs, as visualized by magnetic particle imaging. Overall, our study provides evidence for a highly sensitive assessment of NETosis in lupus through magnetic particle imaging.

## 1. Introduction

Recently, extensive evidence of the oxidative stress-mediated formation of neutrophil extracellular traps (NETs), known as NETosis, has been associated with poorer prognosis in patients with lupus [1, 2, 3] and lung disease [4, 5, 6]. However, it remains a challenge for NETosis detection to discover imaging-based biomarkers.

Biomarker imaging is traditionally understood as imaging of molecular probes. Given the limitations of conventional molecular probes, iron oxide nanoparticles (NP) have been considered as an innovative solution. Recently, injectable NP ferumoxytol has received marketing approval [7]. Immediately, the application of ferumoxytol expanded into lupus diagnosis [8]. It will be interesting for the concept to integrate both molecular biomarkers and NP within new imaging instruments. It may enable a promising new imaging solution, i.e. magnetic particle imaging (MPI) through the application of oscillating magnetic fields for detection and field gradients for localization [9, 10, 11].

We have previously found that a natural mutation in the *Ncf1* gene impairs the formation of the NADPH oxidase 2 (NOX2) complex and the generation of reactive oxygen species (ROS) [1, 12], promotes the proliferation of autoreactive CD4 T cells in spontaneous arthritis [13, 14], enhances autoimmune encephalomyelitis in the absence of inducible nitric oxide [15], promotes the spread of psoriasis through innate production of interleukin 17 (IL-17) [16, 17, 18], activates STAT1 signaling in exaggerated lupus [19], and suppresses NETosis in neutrophils prepared from patients with the chronic granulomatous disease and autoimmune disorders [3, 20]. 147-base pair of NET DNA is typically packed around a histone octamer composed of two copies of each of the histones H3, H4, H2A, and H2B [21]. NET-mediated cytokine induction was observed to depend on H3 citrullination [22], which may provide a new mechanistic paradigm and therapeutic avenue to treat chronic inflammatory diseases. Of importance, NOX2 complex-regulated NETosis was further found in both mouse models and human patients in a nanoparticle size-dependent manner [23, 24, 25]. Therefore, the idea may be interesting to combine both the size-dependent effect and additional NET markers such as Ly6G and H3cit to increase the targeting specificity of NP in tracking lupus.

Here we report the study of anti-Ly6G antibody-conjugated NP (Ly6G-NP) in lupus models using *in vivo* imaging systems. Two models

* Corresponding author.
** Corresponding author.
*E-mail addresses:* jzhong@buaa.edu.cn (J. Zhong), tian@ieee.org (J. Tian).
[1] Lead contact

https://doi.org/10.1016/j.heliyon.2022.e10043
Received 30 June 2021; Received in revised form 15 May 2022; Accepted 18 July 2022

have been developed by C57BL/6J (B6) mice with pristane-induced lupus and B6.MRL-lpr mice with a mutation in the *Fas* gene leading to spontaneous lupus, respectively. We observed a high accumulation of fluorescent Ly6G-NP in the lungs of the lupus mice. The mean fluorescence intensities (MFI) of Ly6G-NP are associated with the expression of citrullinated histone H3 (H3cit), which is a known biomarker for NETosis [19, 20]. The safety of Ly6G-NP was evaluated by examining the level of ROS production in lupus mice. We found lower ROS in the presence of Ly6G-NP using chemiluminescence imaging. The transport of NP from the peritoneal cavity to the lungs was visualized through MPI. Thus, this study provides an approach to the visualization of NETosis in lupus.

## 2. Results

### 2.1. Ly6G-NP imaging associated with NETosis

To comprehensively mimic both NADPH oxidase-dependent and independent ROS signalling that may contribute to NETosis in lupus, we used the NADPH oxidase inhibitor apocynin in a mouse model [26, 27]. The dual-mode scanning of fluorescent Ly6G-NP *in vitro* was performed. Each vial sample contained a volume of 20 $\mu$L. Fluorescence intensity and MPI signal at different concentrations of Ly6G-NP were recorded (Figure 1a and 1b). In the range of 0–25 μg/mL, both the fluorescence intensity ($Y = 1.56 \times 10^5 X + 2.017 \times 10^7$, $R^2 = 0.7441$, $P < 0.05$) and MPI signal ($Y = 0.4378X + 1.367$, $R^2 = 0.8020$, $P < 0.05$) of Ly6G-NP showed a linear correlation with the probe concentration. We intranasally injected 8-week-old B6 mice, with fluorescent Ly6G-NP on 6-day-post-immunization (DPI) of pristane. *In vivo* optical imaging of lupus mice was performed at both 6 h and 24 h after injection of Ly6G-NP into mice. After optical imaging, flow cytometric analysis of both lungs and spleen was performed. The representative graph of fluorescent molecular imaging is shown in Figure 1c. We found a lower radiation efficiency of the lungs from the apocynin-treated mice (Figure 1d and 1e) than that in the control mice receiving phosphate buffer saline (PBS). To better understand the radiation efficiency of Ly6G-NP imaging, the underlying immune responses were analyzed using flow cytometric gating strategies (Figure S1). Compared with control mice, apocynin-treated mice showed lower ROS production (Figure 2a) and H3cit expression (Figure 2b) in splenic neutrophils *ex vivo* after stimulation with phorbol-12-myristate-13-acetate (PMA). It did not affect the level of H3cit expression in splenic monocytes (Figure 2c). These results suggest that fluorescent molecular imaging of Ly6G-NP was associated with NETosis.

### 2.2. NP-induced NETosis

To demonstrate the direct association of NP with NETosis, we collected blood cells from a spontaneous lupus model of B6.MRL-lpr mice. These were analyzed together with healthy individuals from the naïve B6 mice. Blood cells were incubated for 2 h in the presence of unconjugated NP (1 $\mu$g/mL), followed by immunostaining of DNA, H3cit, and Ly6G to qualify NETs (Figure 3a). We found that a strong increase in H3cit expression was induced by NP for samples prepared from lupus mice (Figure 3b).

### 2.3. Oxidative regulation and emigration of Ly6G-NP

To evaluate the neutrophil-dependent effects of Ly6G-NP associated with oxidative stress, we injected it once at a dose of 50 $\mu$g/mouse into the peritoneal cavity of B6 mice at 0 DPI of pristane. *In vivo* small animal imaging was performed using a luminol-based chemiluminescent probe L-012 (1 mg/mouse) every week for one month (Figure 4a). We show decreased production of ROS in the presence of Ly6G-NP at both 7 and 14 DPI of pristane, compared with the control group of mice (Figure 4b). To further validate the emigration of Ly6G-NP and the effect on NETosis, these lupus mice were scanned 24 h after intranasal injection of AF647-conjugated Ly6G-NP (5 $\mu$g/mouse), i.e., 28 DPI of pristane, using dual-modular molecular imaging. We find that these two groups of mice showed similar radiation efficiency of fluorescent Ly6G-NP on the upper

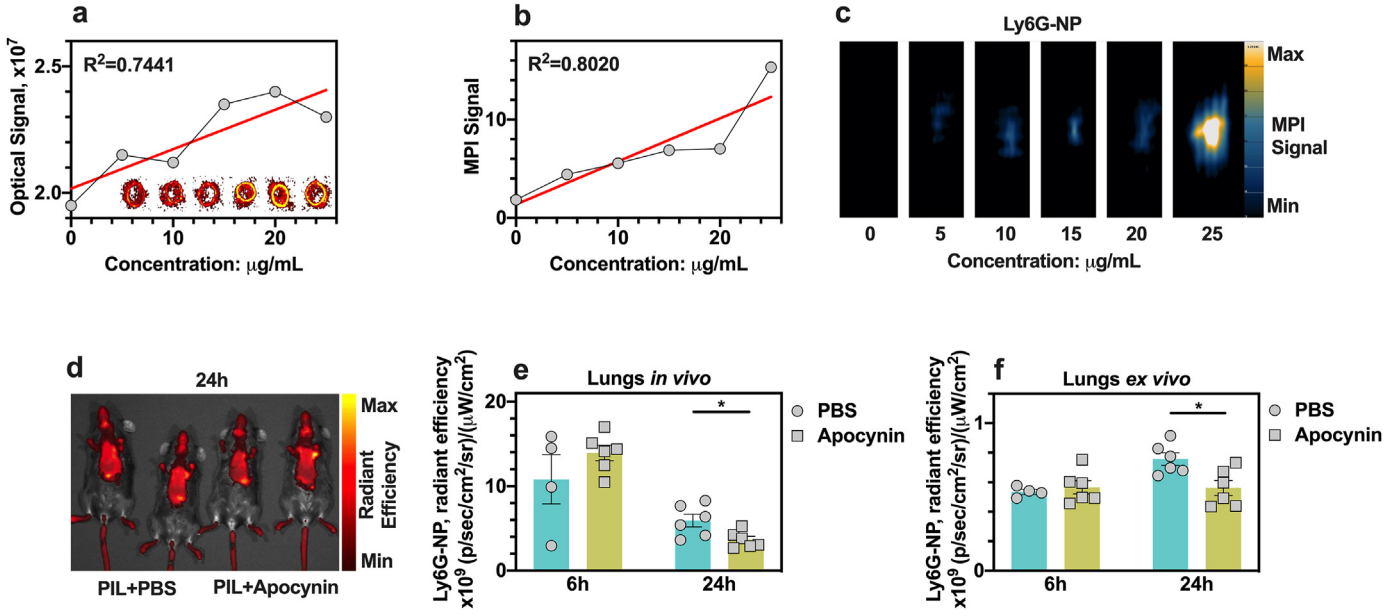


**Figure 1.** Fluorescent molecular imaging of lupus mice. The dual-mode scanning of fluorescent AF647-conjugated Ly6G-NP *in vitro* was performed with six vial samples. a, Optical intensity and, b, MPI signal were recorded, whereas both optical signal ($R^2 = 0.7441$, $P < 0.05$) and MPI signal ($R^2 = 0.8020$, $P < 0.05$) of Ly6G-NP showed a linear correlation with the probe concentration, c, in the range of 0–25 μg/mL. C57BL/6J mice with pristane-induced lupus (PIL) were treated with the NADPH oxidase inhibitor apocynin (5 mmol/L) in drinking water, whereas the same volume of phosphate-buffered saline (PBS) was used as a negative control. Both groups of mice were injected intranasally with the fluorescent Ly6G-NP on 6 day-post-immunization (DPI) of pristane, which was scanned by optical imaging at 6 h and 24 h, respectively. d, A representative graph of optical imaging at 24 h after injection of Ly6G-NP. e, *In vivo* radiant efficiency of Ly6G-NP in the lung region. f, *Ex vivo* radiant efficiency of Ly6G-NP in the lung. Each symbol represents one animal in graph e and f. The mean ± standard error of the mean (SEM) is shown in each graph quoting the P value: $P < 0.05$ *, which is determined by the Mann-Whitney U test.

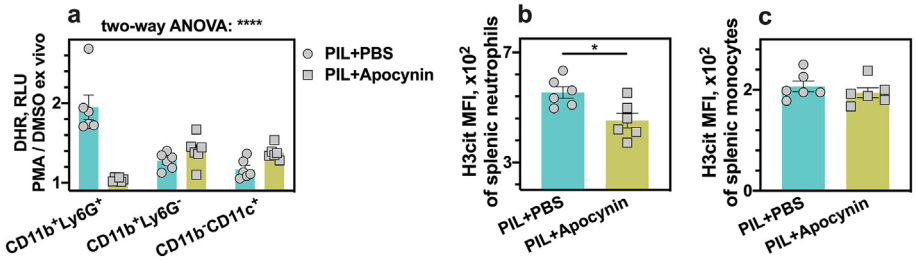


**Figure 2.** ROS production of splenic myeloid cells in lupus mice. PIL mice of C57BL/6J strain were treated with apocynin, while PBS was used as a negative control. Both groups of mice were injected with Ly6G-NP (5 $\mu$ g/mL) at 6 DPI of pristane, and spleen cells were harvested 24 h after injection of Ly6G-NP. Both dihydrorhodamine (DHR) assay and citrullinated histone H3 (H3cit) expression were determined after *ex vivo* stimulation with phorbol-12-myristate-13-acetate (PMA, 100 ng/mL). a, DHR staining of myeloid cells in a relative unit (RLU, DMSO was used as the negative control). b, Mean fluorescence intensities (MFI) of H3cit staining in splenic neutrophils ($CD11b^{+}Ly6G^{+}$). c, MFI of H3cit staining in splenic monocytes ($CD11b^{+}Ly6G^{-}$). Each symbol represents one animal in each graph, and the mean ± standard error of the mean (SEM) is shown. Interaction ****p < 0.0001, row factor *$p < 0.05$, and column factor **$p < 0.01$ as determined by two-way ANOVA test in a. The P value is defined by the Mann-Whitney U test: P < 0.05 * in b.

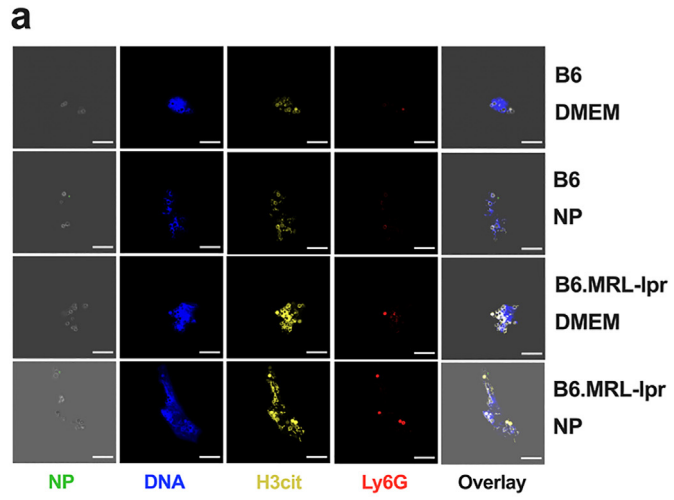


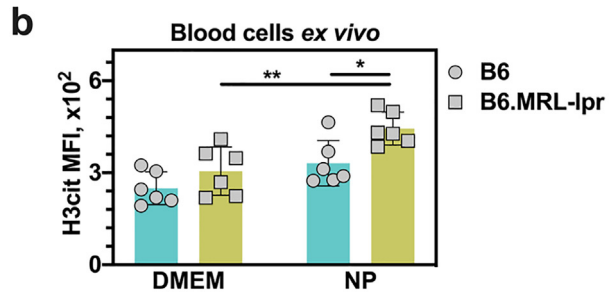


**Figure 3.** Immunostaining of the blood NETs. Blood samples were prepared using B6.*MRL-lpr* lupus-susceptible mice, and H3cit expression was determined after *ex vivo* stimulation with 1 $\mu$ g/mL NP. a, Representative graphs of NETosis in blood cells by using Ly6G, H3cit, and DNA staining. Scale bar indicates 300 $\mu$ m. b, MFI of H3cit staining in NETs. Each symbol represents one animal in each graph, and the mean ± standard error of the mean (SEM) is shown. Row factor ***$p < 0.001$, and column factor **$p < 0.01$ as determined by two-way ANOVA test. The P value is defined by the Mann-Whitney U test: $p < 0.05$ *, $p < 0.01$ **.

surface near the lung (Figure S2), whereas the magnetic signal intensity of the lung was higher in lupus mice receiving Ly6G-NP than in controls (Figure 5a and 5b). These results suggest that Ly6G-NP can be migrated from the peritoneal cavity to the lung and accumulate in the lung for 4 weeks, but they did not affect the detection of dynamic NETosis through a fluorescent molecular probe (Figure 5c).

## 3. Discussion

We report that Ly6G-NP can be used as a molecular imaging probe to monitor NETosis by tracking H3cit expression in priming and chronic phases of lupus through a sensitive MPI scanner.

The dissection of NETs subunits is an area of increasing investigation since NETs were discovered in inflammatory diseases [28, 29, 30]. Recently, a list of common immunologic targets of NETs has been identified in both the cellular and extracellular fluid components of lung samples using proteomic analysis and intravital microscopy imaging. One of the commonly used biomarkers is the expression of H3cit as the origin of the citrullinome in both lupus and lung diseases [19, 31, 32]. Compared with intravital fluorescence microscopy, noninvasively molecular imaging can directly visualize the redox regulation of immune response to stimuli [10, 17, 33]. However, the lack of molecular probes is a problem for NETosis detection [19, 32, 34].

Ferumoxytol is a prescription drug used in the United States to treat iron deficiency anemia and has recently shown promise as a molecular probe in clinical diagnosis [9, 10]. Herrmann and colleagues found that nanoparticles as small as 10 nm size enhance NETosis in a manner dependent on the NOX2 complex-derived ROS [35]. Based on NP of size 14 nm, Chandrasekharan and colleagues used Ly6G-NP at a clinically relevant dose (5–5.5 mg Fe/kg, 40 $\mu$ g protein/mouse) to track neutrophils toward inflammation by magnetic particle imaging [36]. The distribution of Ly6G-NP concentrated in the liver [36].

In this study, we coupled the size-dependent effect of fluorescent NP with the selective recognition ability of anti-Ly6G antibodies (10 nm, 5 $\mu$ g NP conjugated with 2 $\mu$g antibody per mouse) to track neutrophils [37, 38]. Based on this molecular imaging probe of fluorescent Ly6G-NP, we show that fluorescent molecular imaging of lupus mice can quantify NETs. It was successful in noninvasively tracking H3cit expression in the lung, although *in vivo* signals were detected weaker than *ex vivo* signals due to optical absorption properties of tissues. Similar results of lungs displayed with an MPI scanner. One of the most important advantages of MPI is that the linear correction improved between detection signals with a low abundance of NP, compared with fluorescent molecular imaging. However, the liver highlighted as a potential downstream of metabolic pathways for NP.

In summary, our study provides an opportunity to assess noninvasively the NETs formation by tracking H3cit expression in lung disease with Ly6G-NP. Of importance, using Ly6G-NP could protect against oxidative stress in the priming stage of lupus, and did not affect on the re-detection of NETosis after a prolonged period.

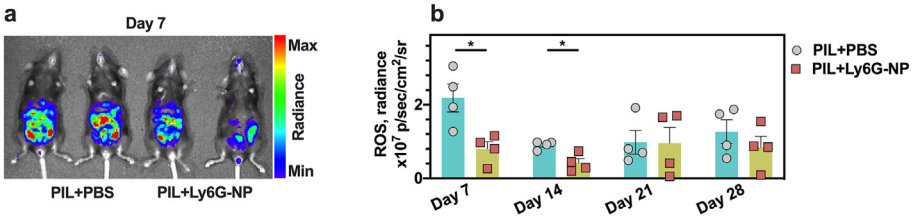


**Figure 4.** Chemiluminescence imaging of lupus mice. Each B6 mouse was administrated intraperitoneally at a dose of 200 $\mu$L with both 50 $\mu$g Ly6G-NP and PBS at 0 DPI of pristane. Production of ROS was detected using a luminol-based molecular imaging probe L-012 (1 mg/mouse) at the indicated time point. a, A representative graph of small animal imaging at 7 DPI of pristane. b, Optical radiance on the top of the abdomen after injection of pristane. Each symbol represents one animal, and the mean ± standard error of the mean (SEM) is shown in b. The P value is defined by the Mann-Whitney U test: $p < 0.05$ *.

### 3.1. Limitations of the study

To the best of our knowledge, it is the first time to visualize non-invasively the NETosis by tracking H3cit with anti-Ly6G iron oxide nanoparticles in a lupus mouse model. In our study, the lupus mice were scanned by fluorescence molecular imaging, showing the accumulation of Ly6G-NP in the lung. This fluorescence molecular imaging was associated with the H3cit expression of neutrophils by flow cytometric analysis. The ROS production was evaluated by chemiluminescent imaging, whereas magnetic particle imaging validates the NP distribution, respectively. However, we observed over 95% of administered NP accumulated in the liver 24 h after injection into the mice. We hypothesized that it is safe for lupus mice with the accumulation of NP. This hypothesis and the potential role of NETs in the liver require further experimental study, despite complementary applications of multimodal molecular imaging.

## 4. Materials and methods

### 4.1. Animals

Founders of B6 (C57BL/6J, Stock No: 000664) and B6.*MRL-lpr* (Stock No: 000482) mice are originally from the JAX Lab (Bar Harbor, Maine) and maintained by the Charles River laboratory (Beijing, China) as inbred lines. The primers for *Fas*$^{lpr}$ genotyping are as following: 5′-TAG AAA GGT GCA CGG GTG TG-3’ (mutant reverse), 5′-GTA AAT AAT TGT GCT TCG TCA G-3’ (common), 5′-CAA ATC TAG GCA TTA ACA GTG-3’ (wild type reverse). Littermate male mice were used in our experiments, and the identity was blinded for the investigator. Mice were housed under specific pathogen-free conditions in individually ventilated cages with wood shaving bedding in a climate-controlled environment having a 12-h light/dark cycle. We have mixed experimental cages of 6- to 8-week-old homozygous littermates. Each adult mouse weighed approximately 25 g. Experimental groups were randomized and distributed among mixed cages. The animal study protocols were approved by animal ethics committee in Beihang University, China (BM20210060).

### 4.2. Antibodies

The following antibodies were purchased from BioLegend, as, CD11b (clone: M1/70, APC), Ly6G (clone: 1A8, PerCP/Cy5.5), Ly-6C (clone: HK1.4, PerCP/Cy5.5), PDC-TREM (clone: 4A6, PE), TCR γ/δ (clone: GL3, PE/Cyanine7), and Ki67 (clone: 16A8, APC). Antibodies for CD16/CD32 (clone: 2.4G2, purified), CD45 (clone: 30-F11, PE-Cyanine7), Gr-1 (clone: RB6-8C5, APC), CD3ε (clone: 145-2C11, PerCP/Cy5.5), CD4 (clone: RM4-5, FITC), B220 (clone: RA3-6B2, PerCP/Cy5.5), MHC II Ap (clone: AF6-120.1, FITC), and IL-17 (clone: TC11-18H10, PE) were purchased from BD Biosciences. Antibodies for H3cit (clone: H3 citrulline R2+R8+R17, Catalog No. ab5103), IgG H&L (goat anti-rabbit, Catalog No. ab175471, PE) were purchased from abcam. Antibodies for Ly6G (clone: 1A8, Biotin) and its isotype control IgG2a were purchased from Leinco Technologies. The use of antibodies is according to the suggestions from the source companies, and the classical dilution ratio of the stock solution is 1:200 for flow cytometry staining.

### 4.3. Pristane induced lupus

Mice were injected intraperitoneally with 300 mL of pristane (Catalog No. P2870, Sigma-Aldrich, US). The presence of serum anti-double stranded DNA (anti-dsDNA) IgG antibody was identified by Crithidia luciliae assay (Catalog No. KMS-H6290C, Kmaels, China).

### 4.4. In vivo optical imaging

Each mouse was injected intraperitoneally with 200 $\mu$L 1.25% avertin (2,2,2-tribromoethanol, Catalog No. T903147-5g, Macklin, China). When mice were anaesthetized, a chemiluminescent prob L-012 (Catalog No. 120-04891, Wako, Tokyo, Japan) was injected with a dose of 1 mg/mouse for the detection of ROS by using bioluminescent imaging model of the IVIS ® Spectrum *in vivo* imaging system (PerkinElmer, Shanghai, China). To perform fluorescent molecular imaging of each mouse, we prepared the fluorescent probe by using the protocol: 5 $\mu$g of AF647-iron oxide nanoparticles-neutravidin (10 nm, Catalog No. CM1, NanoparTZ, Loveland, CO, US) was mixed with 2 $\mu$g anti-Ly6G-biotin antibody in purified water, incubated on the ice for 10 min, and sorted by using the DynaMagTM-15 (Thermofisher, Catalog No. 12301D, Shanghai, China). Each lupus mouse was scanned by using fluorescent molecular imaging model of the IVIS Spectrum imager at 24 h after intranasal administration of 5 $\mu$g fluorescent Ly6G-NP.

### 4.5. Magnetic particle imaging

We used iron oxide nanoparticles-neutravidin with fluorescent dye AF647 (10 nm, Catalog No. CM1, NanoparTZ, Loveland, CO, US) to conjugate anti-Ly6G-biotin antibody at a mass ratio of 5:2. This Ly6G-NP was sorted and injected intraperitoneally in lupus mice at a dose of 50 $\mu$g/mouse, whereas PBS was used as the negative control. On 28 DPI of pristane, i.e., 24 h after intranasal administration of fluorescent Ly6G-NP (2 $\mu$g of antibody conjugated to 5 $\mu$g of NP per mouse), the lungs were harvested. The tissue sample was scanned (MOMENTUM, Magnetic Insight, Alameda, CA, USA) with a magnetic field gradient strength of 6 T/m, a detection limitation of 100 nM NP [10]. Two-dimensional imaging was performed using the following parameters: FOV: 5 × 10 cm; scan mode: isotropic; total time: 2 min. VivoQuant software (VivoQuant 4.0, Invicro, Boston, MA, USA) was used to analyze the images.

### 4.6. Flow cytometry analysis

The single-cell suspensions derived from spleens were analyzed with flow cytometry. Red blood cells were lysed with Ammonium-Chloride-Potassium (ACK) buffer to make single-cell suspensions [18]. Single-cell suspensions of the lymph nodes were generated through 40 $\mu$m filters (Falcon cell strainer, Catalog No. 352340, China) by gravity. The cell density was counted by using EVE automated cell counter (NanoEntek, Seoul, Korea). The cell sample was stained with a LIVE/DEAD® fixable near-IR dead cell stain (ThermoFisher, Catalog No. L10119, China). After an anti-mouse CD16/CD32 Fc block, extracellular antigens were stained 20 min at 4 °C in PBS with 1% fetal bovine serum (FBS, Gibco,

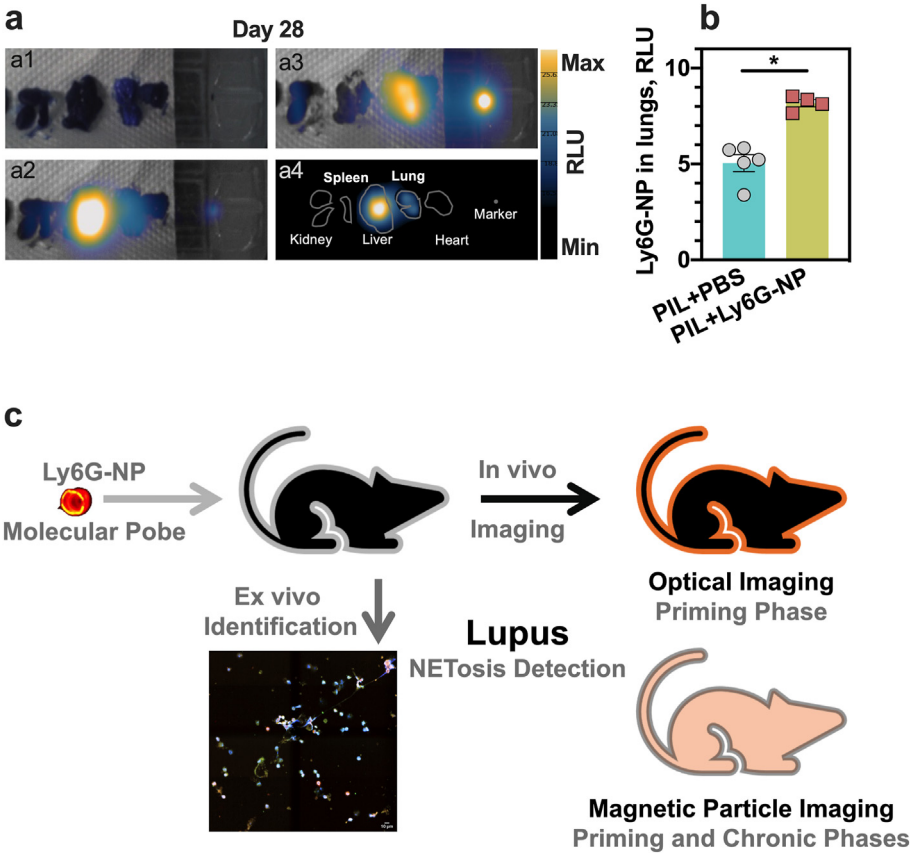


**Figure 5.** Magnetic particle imaging of the inflammatory tissues. Each B6 mouse was administrated intraperitoneally at a dose of 200 $\mu$L with both 50 $\mu$g Ly6G-NP and PBS at 0 DPI of pristane. Fluorescent AF647-conjugated Ly6G-NP (5 $\mu$ g/mouse) was injected intranasally into mice one day before magnetic particle imaging. a, Representative graphs of magnetic particle imaging at 28 DPI of pristane. a1, Tissues (kidney, spleen, liver, lung, and heart) were harvested from a mouse after optical imaging, compared with a standard marker containing 0.1 $\mu$ g Ly6G-NP. a2, Magnetic particle imaging of these tissues; a3, Magnetic particle imaging of. the tissues excluding the liver. a4, Schematic representation of Ly6G-NP distribution in the tissues. b, Statistics of Ly6G-NP distribution in the lung *ex vivo*. Each symbol represents one animal, and the mean ± standard error of the mean (SEM) is shown in b. The P value is defined by the Mann-Whitney U test: $p < 0.05$ *. c, A study scheme of fluorescent Ly6G-NP through dual-modular molecular imaging for NETosis detection in priming and chronic phases of lupus, respectively.

ThermoFisher, Catalog No. 26140079, China). To measure intracellular ROS, the staining of 3 $\mu$M Dihydrorhodamine 123 (DHR, ThermoFisher, Catalog No. D23806, China) was conducted respectively after cell surface markers staining, followed by stimulation of 100 ng/mL of phorbol 12-myristate 13-acetate (PMA, Sigma-Aldrich Co., CAS No. 16561-29-8, China) for 30 min. To detect the intracellular expression of H3cit, the cells were stimulated with 100 ng/mL of phorbol 12-myristate 13-acetate (PMA, Sigma-Aldrich Co., CAS No. 16561-29-8, China) and 1 $\mu$g/mL of ionomycin (ThermoFisher, Catalog No. I24222, China) in the presence of 5 $\mu$g/mL of brefeldin A (BFA, ThermoFisher, Catalog No. B7450, China) for 4 h at a humidified 37 °C, 5% $CO_2$ incubator (BB150, Thermo Scientific, Beijing, China). The stock solutions of PMA, ionomycin, and brefeldin A were prepared with dimethylsulfoxide (DMSO, Sigma-Aldrich Co., CAS No. 67-68-5, China). For intracellular staining of H3cit, cells were fixed and permeabilized by Foxp3/transcription factor fixation/permeabilization concentrate and diluent solutions (eBioscience, Catalog No. 00-5521-00, China) and permeabilization buffer (eBioscience, Catalog No. 00-8333-56, China). Samples were acquired using BD FACSCanto II cell analyzer (BD Biosciences, San Jose, CA, US). The workstation is managed by FACSDiva software version 8.0 (BD Biosciences, San Jose, CA, US), and the data were analysed using the FlowJo software version 10.4 (TreeStar, Ashland, OR, US).

### 4.7. Immunofluorescence microscopy

A blood sample of 30 $\mu$L was collected from the submandibular facial vein for each mouse. Red blood cells were lysed with ammonium-chloride-potassium (ACK) buffer to make single-cell suspensions [18]. To prepare the samples, the glass-coverslip (Jingan, Shanghai, China) was coated with 5 $\mu$g/mL of fibronectin (Sigma, Catalog No. F-0895, China) overnight at 4 °C. To detect NETs, blood cells were incubated in DMEM (gibco, ThermoFisher, Catalog No. A41921, China) for 2 h at a humidified 37 °C, 5% $CO_2$ incubator for them to adhere to the glass-coverslips coated with fibronectin. Blood cells were then treated with 1 $\mu$g/mL of NP (10 nm, Catalog No. CM1, NanoparTZ, Loveland, US) for 2 h at the 5% $CO_2$ incubator in order to trigger NETosis. Furthermore, the cells were stained with the Hoescht 33258 (Blue-absorbing). Then, cells were fixed the cells with 4% paraformaldehyde (Sigma, Catalog No. 158127, China) plus 0.5% glutaraldehyde (Sigma, Catalog No. 6257, China) in PBS (gibco, ThermoFisher, Catalog No. 10010023, China). Samples were blocked with 2% bovine serum albumin (BSA, Sigma, Catalog V900933, China) in PBS, washed by using 1% FBS+0.05% Tween 20 (Sigma, Catalog No. P1379, China) in PBS. After an anti-mouse CD16/CD32 Fc block, extracellular antigens Ly6G were stained 10 min at 4 °C in PBS. Subsequently, samples were incubated with anti-histone 3 citrulline R2+R8+R17 (Abcam), followed by Alexa Fluor 568–conjugated rabbit anti-goat. Samples were mounted in ProLong Gold (ThermoFisher, Catalog No. P36930, China) and examined by Andor Dragonfly 200 confocal microscope (Oxford, Shanghai, China) and analyzed using Fiji/ImageJ software. NET release was quantitated using ImageJ software.

### 4.8. Statistics

Statistical analyses were performed with Graph Prism software, version 8.4.3 (GraphPad Software, San Diego, UAS). Unless otherwise stated, the Mann-Whitney U test was used. A $p$-value less than 0.05 was considered as significant: $^*p < 0.05$ and $^{**}p < 0.01$. The mean ± standard error of the mean (SEM) is shown for all the results.

## Declarations

### Author contribution statement

Jianghong Zhong: Conceived and designed the experiments; Performed the experiments; Analyzed and interpreted the data; Contributed reagents, materials, analysis tools or data; Wrote the paper.

Chanyu Zheng: Performed the experiments; Analyzed and interpreted the data; Contributed reagents, materials, analysis tools or data.

Haiqiang Gao; Wei Tong; Hui Hui: Performed the experiments; Contributed reagents, materials, analysis tools or data.

Jie Tian: Analyzed and interpreted the data; Wrote the paper.

## Funding statement

Jie Tian was supported by National Key Research and Development Program of China [2017YFA0700401] and [2017YFA0700200].

Jie Tian was supported by National Natural Science Foundation of China [62027901] and [81827808].

Hui Hui was supported by Youth Innovation Promotion Association of the Chinese Academy of Sciences [2018167].

Jie Tian was supported by the Project of High-level Talents Team Introduction in Zhuhai city [Zhuhai HLHPTP201703].

Jianghong Zhong was supported by Beihang University [KG160-80401].

## Data availability statement

Data included in article/supp. material/referenced in article.

## Declaration of interest's statement

The authors declare no conflict of interest.

## Additional information

Supplementary content related to this article has been published online at https://doi.org/10.1016/j.heliyon.2022.e10043.

## References

[1] J. Zhong, L.M. Olsson, V. Urbonaviciute, M. Yang, L. Bäckdahl, R. Holmdahl, Association of NOX2 subunits genetic variants with autoimmune diseases, Free Radic. Biol. Med. 125 (2018) 72–80.

[2] J. Zhao, J. Ma, Y. Deng, J.A. Kelly, K. Kim, S.-Y. Bang, H.-S. Lee, Q.-Z. Li, E.K. Wakeland, R. Qiu, M. Liu, J. Guo, Z. Li, W. Tan, A. Rasmussen, C.J. Lessard, K.L. Sivils, B.H. Hahn, J.M. Grossman, D.L. Kamen, G.S. Gilkeson, S.-C. Bae, P.M. Gaffney, N. Shen, B.P. Tsao, A missense variant in NCF1 is associated with susceptibility to multiple autoimmune diseases, Nat. Genet. 49 (2017) 433–437.

[3] L.M. Olsson, Å.C. Johansson, B. Gullstrand, A. Jönsen, S. Saevarsdottir, L. Rönnblom, D. Leonard, J. Wetterö, C. Sjöwall, E. Svenungsson, I. Gunnarsson, A.A. Bengtsson, R. Holmdahl, A single nucleotide polymorphism in the *NCF1* gene leading to reduced oxidative burst is associated with systemic lupus erythematosus, Ann. Rheum. Dis. 76 (2017) 1607–1613.

[4] A. Strangfeld, M. Schäfer, M.A. Gianfrancesco, S. Lawson-Tovey, J.W. Liew, L. Ljung, E.F. Mateus, C. Richez, M.J. Santos, G. Schmajuk, C.A. Scirè, E. Sirotich, J.A. Sparks, P. Sufka, T. Thomas, L. Trupin, Z.S. Wallace, S. Al-Adely, J. Bachiller-Corral, S. Bhana, P. Cacoub, L. Carmona, R. Costello, W. Costello, L. Gossec, R. Grainger, E. Hachulla, R. Hasseli, J.S. Hausmann, K.L. Hyrich, Z. Izadi, L. Jacobsohn, P. Katz, L. Kearsley-Fleet, P.C. Robinson, J. Yazdany, P.M. Machado, Factors associated with COVID-19-related death in people with rheumatic diseases: results from the COVID-19 Global Rheumatology Alliance physician-reported registry, Ann. Rheum. Dis. (2021) 1—13.

[5] Y. Zuo, S.K. Estes, R.A. Ali, A.A. Gandhi, S. Yalavarthi, H. Shi, G. Sule, K. Gockman, J.A. Madison, M. Zuo, V. Yadav, J. Wang, W. Woodard, S.P. Lezak, N.L. Lugogo, S.A. Smith, J.H. Morrissey, Y. Kanthi, J.S. Knight, Prothrombotic autoantibodies in serum from patients hospitalized with COVID-19, Sci. Transl. Med. 12 (2020), eabd3876.

[6] E.A. Middleton, X.-Y. He, F. Denorme, R.A. Campbell, D. Ng, S.P. Salvatore, M. Mostyka, A. Baxter-Stoltzfus, A.C. Borczuk, M. Loda, M.J. Cody, B.K. Manne, I. Portier, E.S. Harris, A.C. Petrey, E.J. Beswick, A.F. Caulin, A. Iovino, L.M. Abegglen, A.S. Weyrich, M.T. Rondina, M. Egeblad, J.D. Schiffman, C.C. Yost, Neutrophil extracellular traps contribute to immunothrombosis in COVID-19 acute respiratory distress syndrome, Blood 136 (2020) 1169–1179.

[7] K.-L. Nguyen, T. Yoshida, N. Kathuria-Prakash, I.H. Zaki, C.G. Varallyay, S.I. Semple, R. Saouaf, C.K. Rigsby, S. Stoumpos, K.K. Whitehead, L.M. Griffin, D. Saloner, M.D. Hope, M.R. Prince, M.A. Fogel, M.L. Schiebler, G.H. Roditi, A. Radjenovic, D.E. Newby, E.A. Neuwelt, M.R. Bashir, P. Hu, J.P. Finn, Multicenter safety and practice for off-label diagnostic use of ferumoxytol in MRI, Radiology 293 (2019) 554–564.

[8] N.J. Serkova, B. Renner, B.A. Larsen, C.R. Stoldt, K.M. Hasebroock, E.L. Bradshaw-Pierce, V.M. Holers, J.M. Thurman, Renal inflammation: targeted iron oxide nanoparticles for molecular MR imaging in mice, Radiology 255 (2010) 517–526.

[9] D.E.J. Waddington, T. Boele, R. Maschmeyer, Z. Kuncic, M.S. Rosen, High-sensitivity in vivo contrast for ultra-low field magnetic resonance imaging using superparamagnetic iron oxide nanoparticles, Sci. Adv. 6 (2020), eabb0998.

[10] W. Tong, H. Hui, W. Shang, Y. Zhang, F. Tian, Q. Ma, X. Yang, J. Tian, Y. Chen, Highly sensitive magnetic particle imaging of vulnerable atherosclerotic plaque with active myeloperoxidase-targeted nanoparticles, Theranostics 11 (2021) 506–521.

[11] P. Chandrasekharan, Z.W. Tay, X.Y. Zhou, E.Y. Yu, B.K.L. Fung, C. Colson, B.D. Fellows, Y. Lu, Q. Huynh, C. Saayujya, P. Keselman, D. Hensley, K. Lu, R. Orendorff, J. Konkle, E.U. Saritas, B. Zheng, P. Goodwill, S. Conolly, Magnetic particle imaging for vascular, cellular and molecular imaging, in: Molecular Imaging, Elsevier, 2021, pp. 265–282.

[12] C. Vingsbo-Lundberg, N. Nordquist, P. Olofsson, M. Sundvall, T. Saxne, U. Pettersson, R. Holmdahl, Genetic control of arthritis onset, severity and chronicity in a model for rheumatoid arthritis in rats, Nat. Genet. 20 (1998) 401–404.

[13] K.A. Gelderman, M. Hultqvist, A. Pizzolla, M. Zhao, K.S. Nandakumar, R. Mattsson, R. Holmdahl, Macrophages suppress T cell responses and arthritis development in mice by producing reactive oxygen species, J. Clin. Invest. 117 (2007) 3020–3028.

[14] J. Zhong, A.C.Y. Yau, R. Holmdahl, Regulation of T Cell function by reactive nitrogen and oxygen species in collagen-induced arthritis, Antioxidants Redox Signal. 32 (2020) 161–172.

[15] J. Zhong, A.C.Y. Yau, R. Holmdahl, Independent and inter-dependent immunoregulatory effects of NCF1 and NOS2 in experimental autoimmune encephalomyelitis, J. Neuroinflammation 17 (2020) 113.

[16] I. Khmaladze, T. Kelkka, S. Guerard, K. Wing, A. Pizzolla, A. Saxena, K. Lundqvist, M. Holmdahl, K.S. Nandakumar, R. Holmdahl, Mannan induces ROS-regulated, IL-17A-dependent psoriasis arthritis-like disease in mice, Proc. Natl. Acad. Sci. U.S.A. 111 (2014) E3669–E3678.

[17] J. Zhong, T. Scholz, A.C.Y. Yau, S. Guerard, U. Hüffmeier, H. Burkhardt, R. Holmdahl, Mannan-induced Nos2 in macrophages enhances IL-17–driven psoriatic arthritis by innate lymphocytes, Sci. Adv. 4 (2018), eaas9864.

[18] J. Zhong, Q. Li, R. Holmdahl, Natural loss-of-function mutations in Qa2 and NCF1 cause the spread of mannan-induced psoriasis, J. Invest. Dermatol. 141 (2021) 1765–1771, e4.

[19] D. Kienhöfer, J. Hahn, J. Stoof, J.Z. Csepregi, C. Reinwald, V. Urbonaviciute, C. Johnsson, C. Maueröder, M.J. Podolska, M.H. Biermann, M. Leppkes, T. Harrer, M. Hultqvist, P. Olofsson, L.E. Munoz, A. Mocsai, M. Herrmann, G. Schett, R. Holmdahl, M.H. Hoffmann, Experimental lupus is aggravated in mouse strains with impaired induction of neutrophil extracellular traps, JCI Insight 2 (2017), e92920.

[20] C. Schauer, C. Janko, L.E. Munoz, Y. Zhao, D. Kienhöfer, B. Frey, M. Lell, B. Manger, J. Rech, E. Naschberger, R. Holmdahl, V. Krenn, T. Harrer, I. Jeremic, R. Bilyy, G. Schett, M. Hoffmann, M. Herrmann, Aggregated neutrophil extracellular traps limit inflammation by degrading cytokines and chemokines, Nat. Med. 20 (2014) 511–517.

[21] Y. Wang, M. Li, S. Stadler, S. Correll, P. Li, D. Wang, R. Hayama, L. Leonelli, H. Han, S.A. Grigoryev, C.D. Allis, S.A. Coonrod, Histone hypercitrullination mediates chromatin decondensation and neutrophil extracellular trap formation, J. Cell Biol. 184 (2009) 205–213.

[22] T.-D. Tsourouktsoglou, A. Warnatsch, M. Ioannou, D. Hoving, Q. Wang, V. Papayannopoulos, Histones, DNA, and citrullination promote neutrophil extracellular trap inflammation by regulating the localization and activation of TLR4, Cell Rep. 31 (2020), 107602.

[23] L.E. Muñoz, R. Bilyy, M.H.C. Biermann, D. Kienhöfer, C. Maueröder, J. Hahn, J.M. Brauner, D. Weidner, J. Chen, M. Scharin-Mehlmann, C. Janko, R.P. Friedrich, D. Mielenz, T. Dumych, M.D. Lootsik, C. Schauer, G. Schett, M. Hoffmann, Y. Zhao, M. Herrmann, Nanoparticles size-dependently initiate self-limiting NETosis-driven inflammation, Proc. Natl. Acad. Sci. U.S.A. 113 (2016) E5856. –E5865.

[24] L.E. Muñoz, S. Boeltz, R. Bilyy, C. Schauer, A. Mahajan, N. Widulin, A. Grüneboom, I. Herrmann, E. Boada, M. Rauh, V. Krenn, M.H.C. Biermann, M.J. Podolska, J. Hahn, J. Knopf, C. Maueröder, S. Paryzhak, T. Dumych, Y. Zhao, M.F. Neurath, M.H. Hoffmann, T.A. Fuchs, M. Leppkes, G. Schett, M. Herrmann, Neutrophil extracellular traps initiate gallstone formation, Immunity 51 (2019) 443–450.e4.

[25] M.H.C. Biermann, M.J. Podolska, J. Knopf, C. Reinwald, D. Weidner, C. Maueröder, J. Hahn, D. Kienhöfer, A. Barras, R. Boukherroub, S. Szunerits, R. Bilyy, M. Hoffmann, Y. Zhao, G. Schett, M. Herrmann, L.E. Munoz, Oxidative burst-dependent NETosis is implicated in the resolution of necrosis-associated sterile inflammation, Front. Immunol. 7 (2016).

[26] M. Mora-Pale, S. Joon Kwon, R.J. Linhardt, J.S. Dordick, Trimer hydroxylated quinone derived from apocynin targets cysteine residues of p47phox preventing the activation of human vascular NADPH oxidase, Free Radical Biol. Med. 52 (2012) 962–969.

[27] C. Lood, L.P. Blanco, M.M. Purmalek, C. Carmona-Rivera, S.S. De Ravin, C.K. Smith, H.L. Malech, J.A. Ledbetter, K.B. Elkon, M.J. Kaplan, Neutrophil extracellular traps enriched in oxidized mitochondrial DNA are interferogenic and contribute to lupus-like disease, Nat. Med. 22 (2016) 146–153.

[28] V. Brinkmann, Neutrophil extracellular traps kill bacteria, Science 303 (2004) 1532–1535.

[29] J. Fert-Bober, E. Darrah, F. Andrade, Insights into the study and origin of the citrullinome in rheumatoid arthritis, Immunol. Rev. 294 (2020) 133–147.

[30] J.S. Knight, V. Subramanian, A.A. O'Dell, S. Yalavarthi, W. Zhao, C.K. Smith, J.B. Hodgin, P.R. Thompson, M.J. Kaplan, Peptidylarginine deiminase inhibition disrupts NET formation and protects against kidney, skin and vascular disease in lupus-prone MRL/*lpr* mice, Ann. Rheum. Dis. 74 (2015) 2199–2206.

[31] A.M. Billing, K.B. Knudsen, A.J. Chetwynd, L.-J.A. Ellis, S.V.Y. Tang, T. Berthing, H. Wallin, I. Lynch, U. Vogel, F. Kjeldsen, Fast and robust proteome screening

platform identifies neutrophil extracellular trap formation in the lung in response to cobalt ferrite nanoparticles, ACS Nano 14 (2020) 4096–4110.
[32] J.M. Adrover, A. Aroca-Crevillén, G. Crainiciuc, F. Ostos, Y. Rojas-Vega, A. Rubio-Ponce, C. Cilloniz, E. Bonzón-Kulichenko, E. Calvo, D. Rico, M.A. Moro, C. Weber, I. Lizasoaín, A. Torres, J. Ruiz-Cabello, J. Vázquez, A. Hidalgo, Programmed 'disarming' of the neutrophil proteome reduces the magnitude of inflammation, Nat. Immunol. 21 (2020) 135–144.
[33] H.R. Herschman, Molecular imaging: looking at problems, seeing solutions, Science 302 (2003) 605–608.
[34] J. Zhong, J. Tian, X. Yang, C. Qin, Whole-body cerenkov luminescence tomography with the finite element SP3 method, Ann. Biomed. Eng. 39 (2011) 1728–1735.
[35] L.E. Muñoz, R. Bilyy, M.H.C. Biermann, D. Kienhöfer, C. Maueröder, J. Hahn, J.M. Brauner, D. Weidner, J. Chen, M. Scharin-Mehlmann, C. Janko, R.P. Friedrich, D. Mielenz, T. Dumych, M.D. Lootsik, C. Schauer, G. Schett, M. Hoffmann, Y. Zhao, M. Herrmann, Nanoparticles size-dependently initiate self-limiting NETosis-driven inflammation, Proc. Natl. Acad. Sci. U.S.A. 113 (2016). E5856–E5865.
[36] P. Chandrasekharan, K.L.B. Fung, X.Y. Zhou, W. Cui, C. Colson, D. Mai, K. Jeffris, Q. Huynh, C. Saayujya, L. Kabuli, B. Fellows, Y. Lu, E. Yu, Z.W. Tay, B. Zheng, L. Fong, S.M. Conolly, Non-radioactive and sensitive tracking of neutrophils towards inflammation using antibody functionalized magnetic particle imaging tracers, Nanotheranostics 5 (2021) 240–255.
[37] F.C. Weber, T. Németh, J.Z. Csepregi, A. Dudeck, A. Roers, B. Ozsvári, E. Oswald, L.G. Puskás, T. Jakob, A. Mócsai, S.F. Martin, Neutrophils are required for both the sensitization and elicitation phase of contact hypersensitivity, J. Exp. Med. 212 (2015) 15–22.
[38] G. Boivin, J. Faget, P.-B. Ancey, A. Gkasti, J. Mussard, C. Engblom, C. Pfirschke, C. Contat, J. Pascual, J. Vazquez, N. Bendriss-Vermare, C. Caux, M.-C. Vozenin, M.J. Pittet, M. Gunzer, E. Meylan, Durable and controlled depletion of neutrophils in mice, Nat. Commun. 11 (2020) 2762.